Electronic Supplementary Material (ESI) for New Journal of Chemistry.

Supporting Information

Low-coordinated Pd metallene promotes electrochemical reduction of nitrite to ammonia

Wenhuan Qu [a], Tingting Wu [a], Jingxuan Wang [a], Xiaoxu Liu[a], Ye Tian [a], Ke Chu[b]**

[a] *College of Science, Hebei North University, Zhangjiakou 075000, Hebei, China*

[b] *School of Materials Science and Engineering, Lanzhou Jiaotong University, Lanzhou 730070, China*

**Corresponding author. qwenhuan2023@163.com (W.H. Qu), chuk630@mail.lzjtu.cn (K. Chu)*

Experimental Section

Synthesis of L-Pd

All the reagents were of analytical grade and were used as received without further purification. To prepare Pd metallene, 0.25 g of trinoctylphosphine oxide and 20 mg of $Pd(acac)_2$ were dissolved in octanoic acid (OA) and kept at 60 ^oC in an oil bath. The mixed solution was then added with 5 mL of DMF and 20 mg of $Mo(CO)_6$ and kept for 1 h. The precipitates were collected via centrifugation, thoroughly rinsed with deionized water and dried overnight. The obtained Pd metallene was further subjected to Ar plasma treatment for 5 min in an AX-1000 plasma system (13.56 MHz) to obtain low-coordinated Pd metallene (L-Pd).

Electrochemical experiments and characterizations

Electrochemical measurements were carried out using a CHI-760E electrochemical workstation employing a three-electrode cell system consisting of a working electrode, an Ag/AgCl reference electrode and a Pt foil counter electrode. The working electrode is L-Pd catalyst loaded on pretreated carbon cloth (CC). The CC (1 × 1 cm^2) was pretreated by soaking it in 0.5 M H_2SO_4 for 12 h, and then washed with deionized water several times and dried at 60 ℃ for 24 h. The working electrode was prepared by coating 20 μL of the catalyst ink onto the pretreated CC and dried in the air. The catalyst ink was fabricated by ultrasonically dispersing 1 mg of the catalyst in 100 μL of ethyl alcohol containing 5 μL of Nafion (5 wt%). All the potentials were referenced to a reversible hydrogen electrode (RHE) by the following equation: E (V vs. RHE) = E (V vs. Ag/AgCl) + 0.198 V + 0.059 × pH. Electrochemical NO_2RR measurements were conducted in an H-type electrochemical cell containing 0.5 M Na_2SO_4 with 0.1 M $NaNO_2$ separated by Nafion 211 membrane. Prior to use, the Nafion membrane was pretreated by heating it in a 5% H_2O_2 aqueous solution at 80 °C for 1 h, followed by rinsing with deionized water at 80 °C for another 1 h. After each chronoamperometry test for 0.5 h electrolysis at a specific potential, the liquid products were analyzed using colorimetric methods with UV-vis absorbance spectrophotometer (MAPADA P5), while the gas products were analyzed

using gas chromatography (Shimadzu GC2010). Transmission electron microscopy (TEM) was conducted on a Tecnai G^2 F20 microscope. X-ray diffraction (XRD) was carried out on a Rigaku D/max 2400 diffractometer. Atom force microscopy (AFM) was performed on a Nanoscope-IIIa scanning probe microscope.

Determination of NH_3

The NH_3 concentration in the electrolyte was determined using the an indophenol blue method[1]. The electrolyte was collected and appropriately diluted to ensure it fell within the detection range. In a typical colorimetric assay, 2 mL of the diluted electrolyte obtained after electrolysis were mixed with 1 mL of NaClO solution (4.5%), 2 mL of 1 M NaOH solution (containing 5% $C_7H_6O_3$ and 5% $C_6H_5Na_3O_7{\cdot}2H_2O$), and 0.2 mL of a mixed solution (prepared by diluting 1 g $Na_2Fe(CN)_5NO{\cdot}2H_2O$ to 100 mL using ultrapure water). The mixture was allowed to stand for 2 h, after which UV-vis absorption spectra were measured. The concentration-absorbance curves were calibrated using a standard NH_4Cl solution with various concentrations. The NH_3 yield rate and FE_{NH3} (Faradaic efficiency of NH_3 production) were calculated using the following equation:

NH_3 yield was calculated by

$$\mathrm{NH_3\ yield\ (\mu g\ h^{-1}\ cm^{-2})} = \frac{c_{\mathrm{NH_3}} \times V}{t \times A} \tag{1}$$

FE_{NH3} was calculated by

$$\mathrm{FE_{NH3}(\%)} = \frac{6 \times F \times c_{\mathrm{NH_3}} \times V}{M \times Q} \times 100\% \tag{2}$$

where c_{NH3} (μg mL^{-1}) is the measured NH_3 concentration, V (mL) is the volume of the electrolyte, t (h) is the reduction time and A (cm^{-2}) is the area loading of the catalyst on CC. F (96500 C mol^{-1}) is the Faraday constant, M is the relative molecular mass of NH_3, Q is the quantity of applied electricity.

Calculation details

Density functional theory (DFT) calculations were conducted using a Cambridge sequential total energy package (CASTEP). The method of the Perdew-Burke-Ernzerhof (PBE) generalized gradient approximation (GGA) functional was utilized

for the exchange-correlation potential. The DFT-D correction method was used to describe the van der Waals interactions. A cutoff energy of 450 eV was chosen and the 3×3×1 Monkhorst-Pack mesh was used in Brillouin zone sampling. Energy and force will not reach convergence until lower to 1.0×10^{-5} eV and 0.02 eV/Å, respectively. Pd (111) was modeled by a 4×4 supercell, and a vacuum region of 15 Å was used to separate adjacent slabs.

The computational hydrogen electrode (CHE) model was adopted to calculate the Gibbs free energy change (ΔG) for each elementary step as follows[3]:

$$\Delta G = \Delta E + \Delta E_{ZPE} - T\Delta S \tag{3}$$

where ΔE is the adsorption energy, ΔE_{ZPE} is the zero-point energy difference and $T\Delta S$ is the entropy difference between the gas phase and adsorbed state. The entropies of free gases were acquired from the NIST database.

MD simulations were performed using a force field type of Universal. The electrolyte system was modeled by a cubic cell with placing catalyst at the center of the cell and randomly filling 1000 H_2O, 50 NO_2^- molecules, and 50 H atoms. After geometry optimization, the MD simulations were performed in an NVT ensemble (298 K) with the total simulation time of 5 ns at a time step of 1 fs.

The radial distribution function (RDF) is calculated by[3]:

$$g(r) = \frac{dN}{4\pi\rho r^2 dr} \tag{4}$$

where dN is the amount of NO_2^- in the shell between the central particle r and $r+dr$, ρ is the number density of NO_2^-, H_2O, and H.

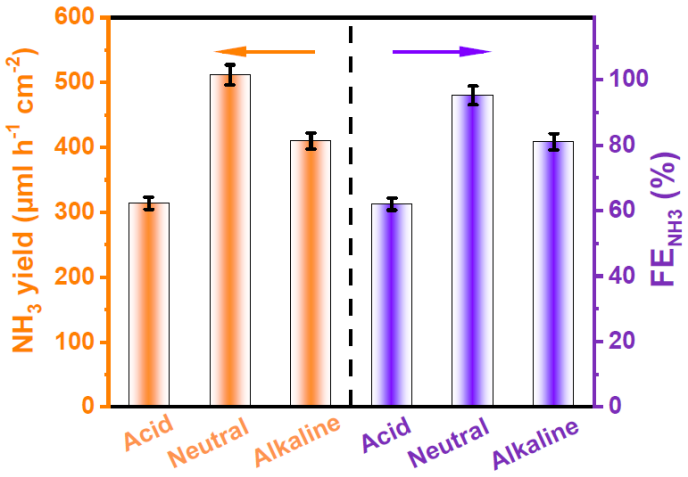

Fig. S1. Comparison of the NO_2RR performances of L-Pd in acidic, neutral, and alkaline electrolytes at -0.6 V.

It is shown that L-Pd shows a significantly enhanced NO_2RR activity in neutral electrolyte compared to that in acidic and basic electrolytes, demonstrating the superiority of neutral electrolyte in facilitating the high NO_2RR performance. The reduced performance in acidic and basic electrolytes is attributed to the fact that in acid electrolyte, the competing HER would be enhanced and can largely suppress the NO_2RR, while in alkaline electrolyte, the available protons are too limited to provide the sufficient proton source for hydrogenating nitrogen species during the NO_2RR electrolysis, because NO_2^--to-NH_3 conversion is known to be a hydrogenation process.

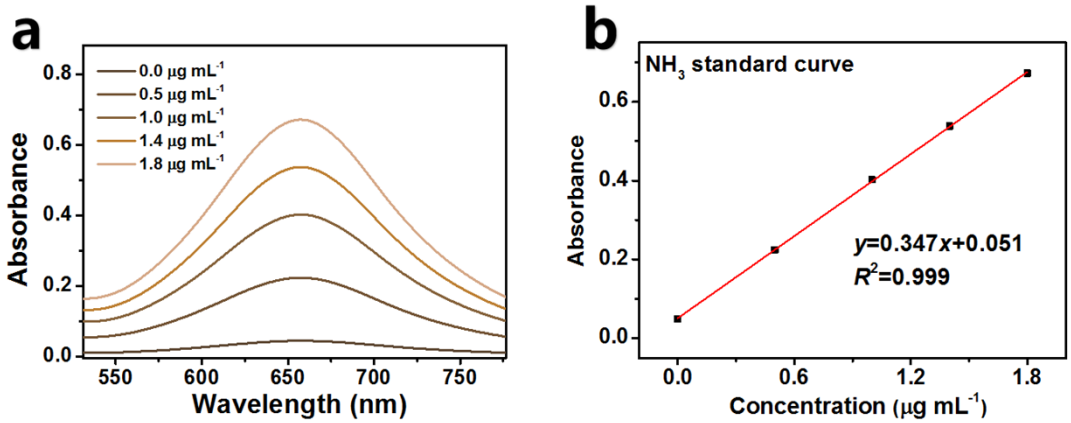

Fig. S2. (a) UV-vis absorption spectra of NH_4^+ assays after incubated for 2 h at ambient conditions. (b) Calibration curve used for the calculation of NH_3 concentrations.

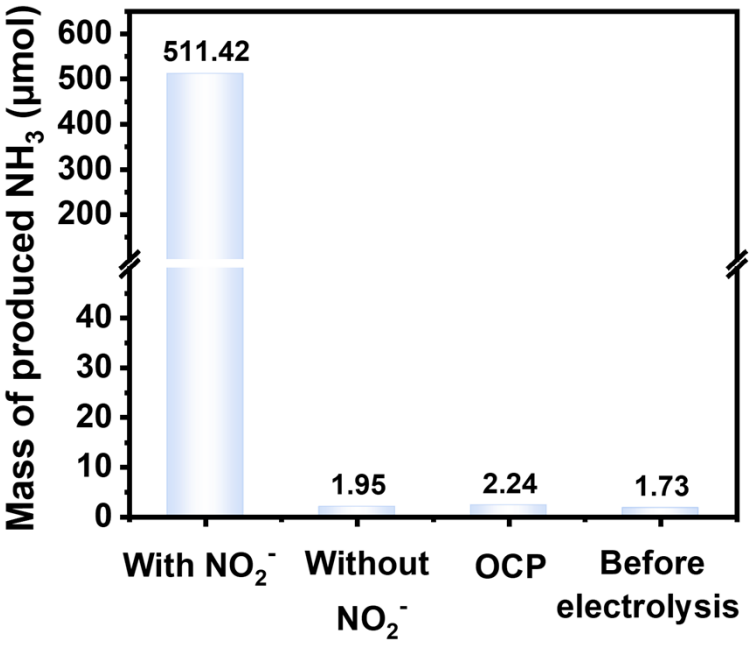

Fig. S3. Amounts of produced NH_3 on L-Pd under different conditions: (1) electrolysis in NO_2^--containing solution at -0.8 V, (2) electrolysis in NO_2^--free solution at -0.8 V, (3) electrolysis in NO_2^--containing solution at open-circuit potential (OCP), (4) before electrolysis.

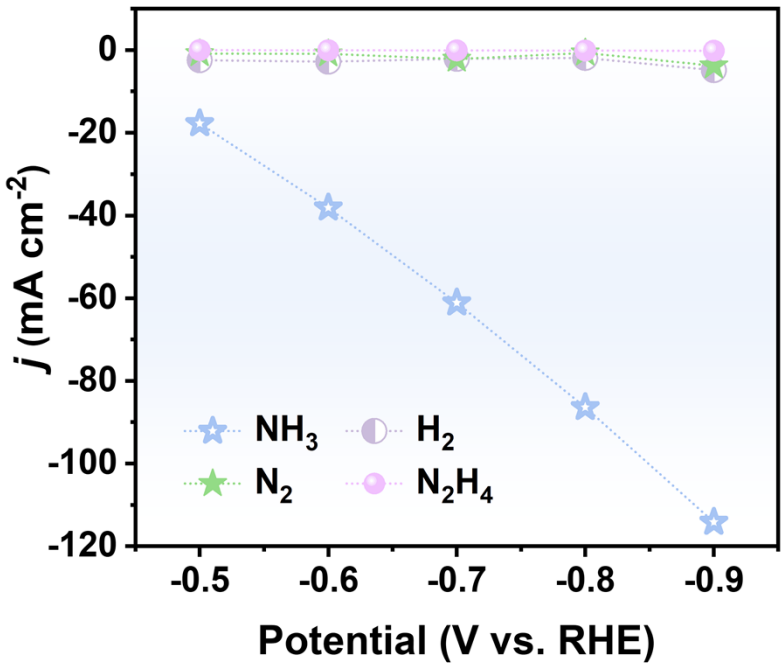

Fig. S4. Partial current densities of various products over L-Pd after 0.5 h of NO_2RR electrolysis at different potentials.

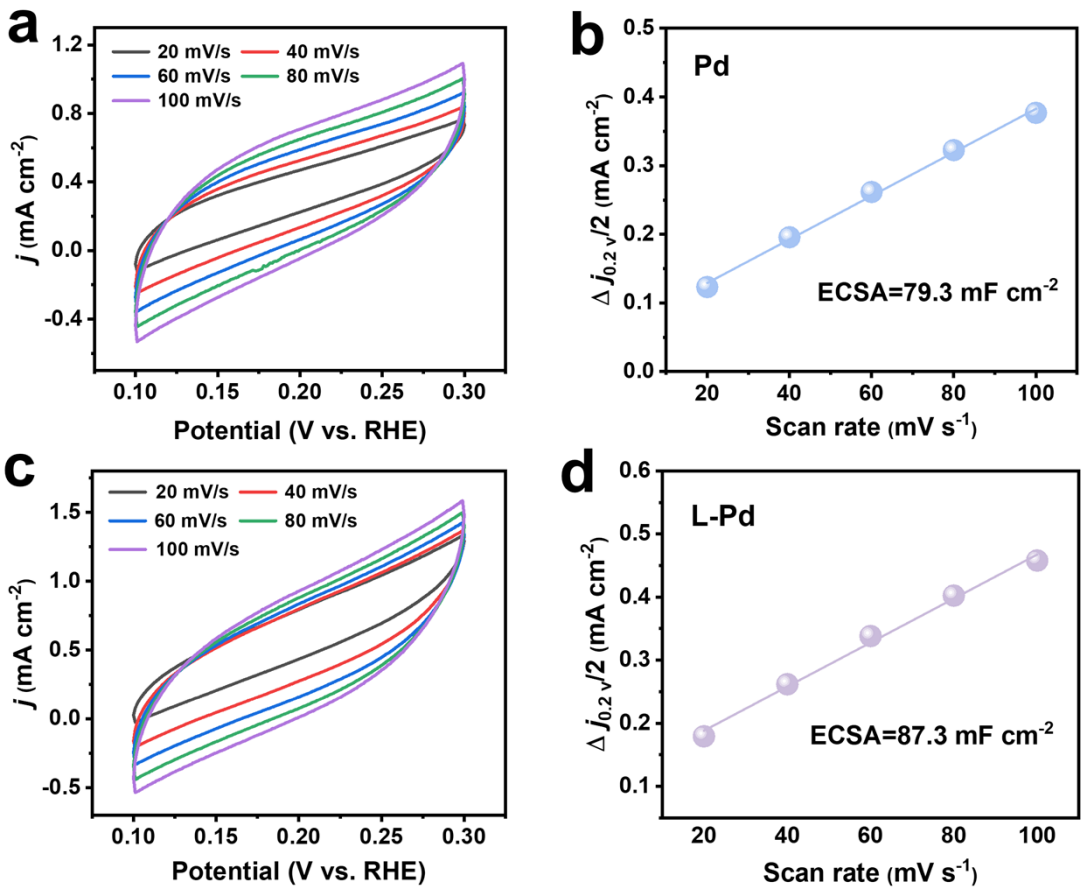

Fig. S5. CV measurements in 0.5 M Na_2SO_4 electrolyte at different scanning rates for (a, b) Pd and (c, d) L-Pd, and corresponding calculated ECSA.

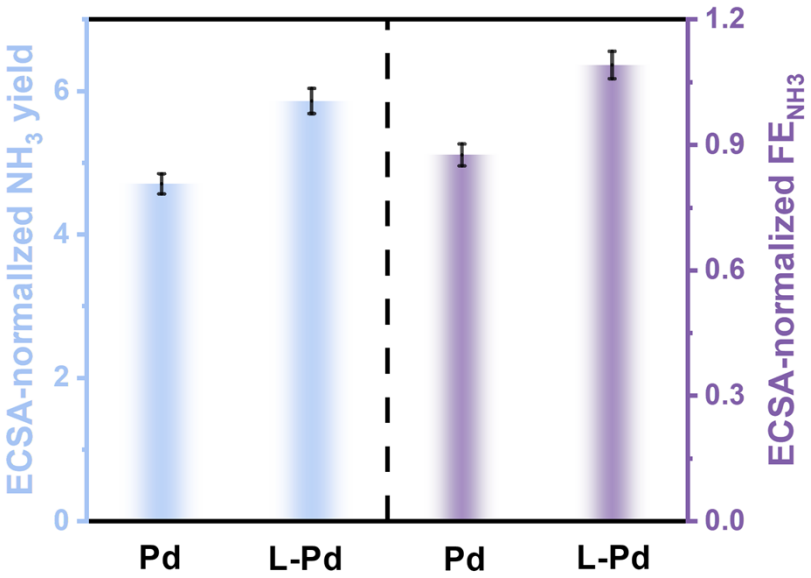

Fig. S6. Comparison of the ECSA-normalized NH_3 yield rates and FE_{NH3} between Pd and L-Pd at -0.8 V.

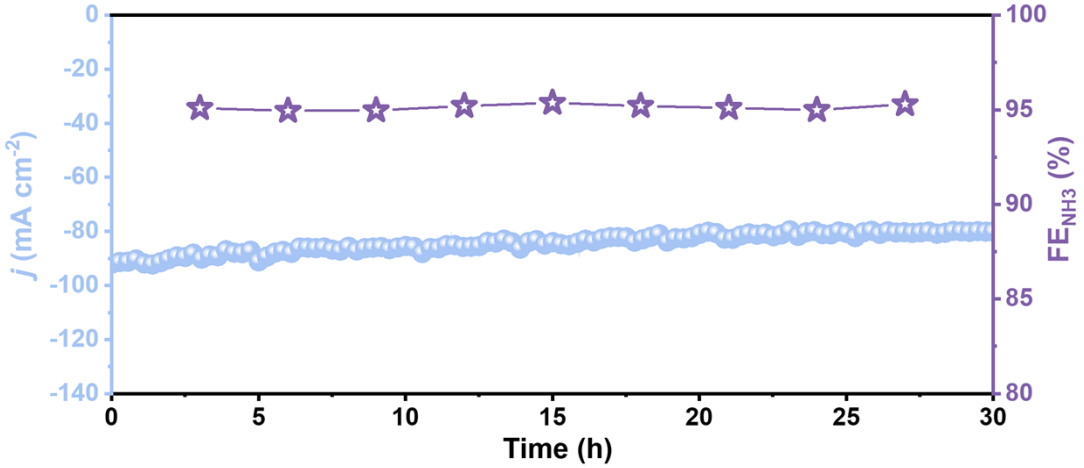

Fig. S7. Long-term chronoamperometry test of L-Pd at -0.8 V.

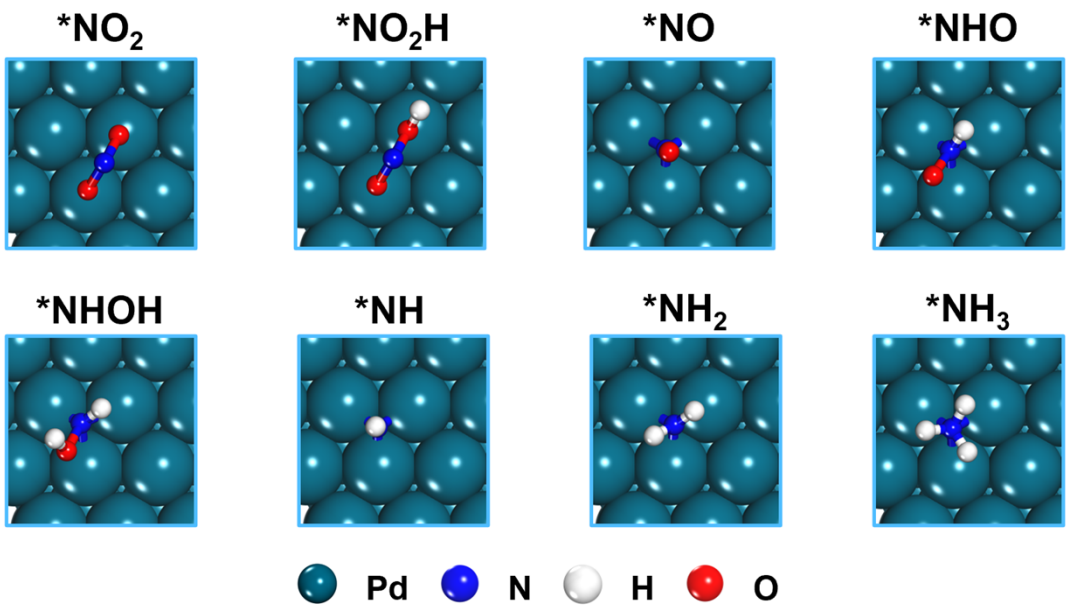

Fig. S8. Optimized atomic configurations of the NO_2RR reaction intermediates on Pd.

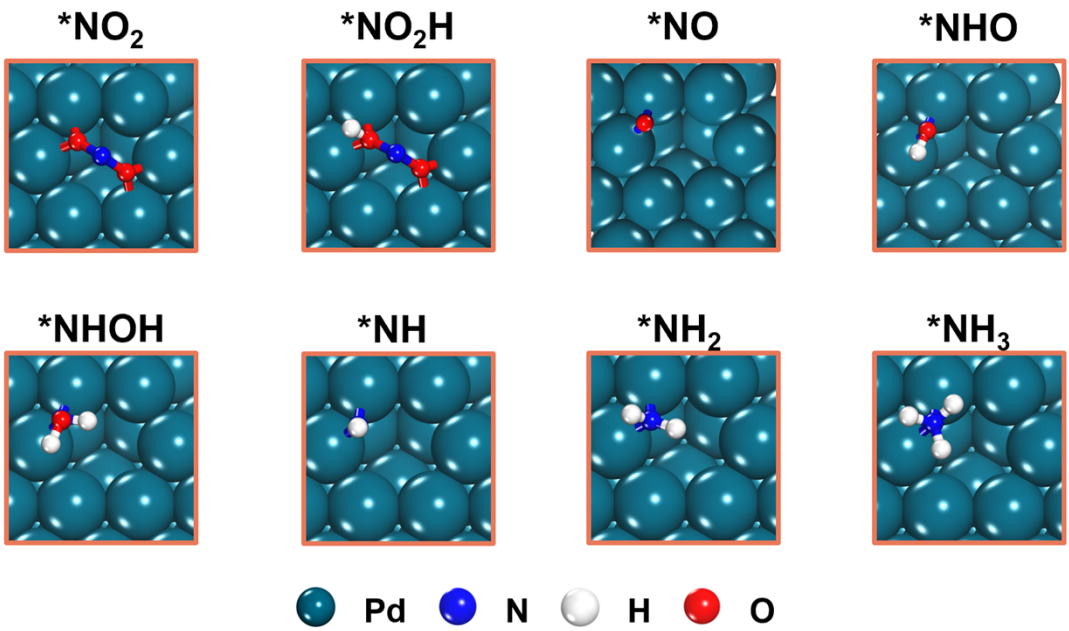

Fig. S9. Optimized atomic configurations of the NO_2RR reaction intermediates on L-Pd.

Table S1. Comparison of the optimum NH_3 yield rate and NH_3-Faradic efficiency (FE_{NH3}) for the recently reported NO_2RR electrocatalysts at ambient conditions

Catalyst	Electrolyte	NH_3 yield rate ($mg\ h^{-1}\ cm^{-2}$)	FE_{NH3}	Reference
P-TiO_2/TP	0.1 M Na_2SO_4 (0.1 M NO_2^-)	560.8	90.6%@-0.6 V	[4]
CoB@TiO_2/TP	0.1 M Na_2SO_4 (400 ppm NO_2^-)	233.1	95.2%@−0.7 V	[5]
Ag@NiO/CC	0.1 M NaOH (0.1 M NO_2^-)	338.3	96.1%@-0.7 V	[6]
Ni_2P/NF	0.1 M PBS (200 ppm NO_2^-)	191.3	90.2±3.0% @-0.3 V	[7]
CF@Cu_2O	0.1 M PBS (0.1 M NO_2^-)	441.8	94.2% @-0.6 V	[8]
V-TiO_2/TP	0.1 M NaOH (0.1 M NO_2^-)	540.8	93.2% @-0.6 V	[9]
CoP NA/TM	0.1 M PBS (500 ppm NO_2^-)	132.7±3.0	90±2.3% @-0.2 V	[10]
Ni-TiO_2/TP	0.1 M NaOH (0.1 M NO_2^-)	380.27	94.89% @-0.5 V	[11]
NiS_2@TiO_2/TM	0.1 M NaOH (0.1 M NO_2^-)	485.4	92.1% @-0.5 V	[12]
L-Pd	**0.5 M Na_2SO_4 (0.1 M NO_2^-)**	**511.5**	**95.2% @-0.8 V**	**This work**

References

[1]. D. Zhu, L. Zhang, R. E. Ruther and R. J. Hamers, *Nat. Mater.*, 2013, **12**, 836-841.

[2]. G. W. Watt and J. D. Chrisp, *Anal. Chem.*, 1952, **24**, 2006-2008.

[3]. X. Li, P. Shen, Y. Luo, Y. Li, Y. Guo, H. Zhang and K. Chu, *Angew. Chem. Int. Edit.*, 2022, **134**, e202205923.

[4]. L. Ouyang, X. He, S. Sun, Y. Luo, D. Zheng, J. Chen, Y. Li, Y. Lin, Q. Liu, A. M. Asiri and X. Sun, *J. Mater. Chem. A*, 2022, **10**, 23494-23498.

[5]. L. Hu, D. Zhao, C. Liu, Y. Liang, D. Zheng, S. Sun, Q. Li, Q. Liu, Y. Luo, Y. Liao, L. Xie and X. Sun, *Inorg. Chem. Front.*, 2022, **9**, 6075-6079.

[6]. Q. Liu, G. Wen, D. Zhao, L. Xie, S. Sun, L. Zhang, Y. Luo, A. Ali Alshehri, M. S. Hamdy, Q. Kong and X. Sun, *J. Colloid Interf. Sci.*, 2022, **623**, 513-519.

[7]. G. Wen, J. Liang, L. Zhang, T. Li, Q. Liu, X. An, X. Shi, Y. Liu, S. Gao, A. M. Asiri, Y. Luo, Q. Kong and X. Sun, *J. Colloid Interf. Sci.*, 2022, **606**, 1055-1063.

[8]. Q. Chen, X. An, Q. Liu, X. Wu, L. Xie, J. Zhang, W. Yao, M. S. Hamdy, Q. Kong and X. Sun, *Chem. Commun.*, 2022, **58**, 517-520.

[9]. H. Wang, F. Zhang, M. Jin, D. Zhao, X. Fan, Z. Li, Y. Luo, D. Zheng, T. Li, Y. Wang, B. Ying, S. Sun, Q. Liu, X. Liu and X. Sun, *Mater. Today Phys.*, 2023, **30**, 100944.

[10]. G. Wen, J. Liang, Q. Liu, T. Li, X. An, F. Zhang, A. A. Alshehri, K. A. Alzahrani, Y. Luo, Q.

Kong and X. Sun, *Nano Res.*, 2022, **15**, 972-977.
[11]. Z. Cai, C. Ma, D. Zhao, X. Fan, R. Li, L. Zhang, J. Li, X. He, Y. Luo, D. Zheng, Y. Wang, B. Ying, S. Sun, J. Xu, Q. Lu and X. Sun, *Mater. Today Energy*, 2023, **31**, 101220.
[12]. X. He, L. Hu, L. Xie, Z. Li, J. Chen, X. Li, J. Li, L. Zhang, X. Fang, D. Zheng, S. Sun, J. Zhang, A. Ali Alshehri, Y. Luo, Q. Liu, Y. Wang and X. Sun, *J. Colloid Interface Sci.*, 2023, **634**, 86-92.